A thermo-sensitive chitosan/pectin hydrogel for long-term tumor spheroid culture

Carbohydrate Polymers 274 (2021) 118633

Contents lists available at ScienceDirect

Carbohydrate Polymers

journal homepage: www.elsevier.com/locate/carbpol

A thermo-sensitive chitosan/pectin hydrogel for long-term tumor spheroid culture

Giulia Morello [a,b], Alessandra Quarta [a], Antonio Gaballo [a], Lorenzo Moroni [a,c], Giuseppe Gigli [a,b], Alessandro Polini [a,*,1], Francesca Gervaso [a,*,1]

[a] Institute of Nanotechnology, CNR, Lecce 73100, Italy
[b] Dipartimento di Matematica e Fisica E. de Giorgi, Università Del Salento, Lecce 73100, Italy
[c] Department of Complex Tissue Regeneration, MERLN Institute for Technology-Inspired Regenerative Medicine, Maastricht University, Maastricht 6229ER, the Netherlands

ARTICLE INFO

Keywords:
Natural polymers
Thermo-responsive hydrogels
Semi-IPN
In vitro tumor models
Colorectal cancer
CRC spheroids
Tumor microenvironment

ABSTRACT

Hydrogels represent a key element in the development of *in vitro* tumor models, by mimicking the typical 3D tumor architecture in a physicochemical manner and allowing the study of tumor mechanisms. Here we developed a thermo-sensitive, natural polymer-based hydrogel, where chitosan and pectin were mixed and, after a weak base-induced chitosan gelation, a stable semi-Interpenetrating Polymer Network formed. This resulted thermo-responsive at 37 °C, injectable at room temperature, stable up to 6 weeks *in vitro*, permeable to small/medium-sized molecules (3 to 70 kDa) and suitable for cell-encapsulation. Tunable mechanical and permeability properties were obtained by varying the polymer content. Optimized formulations successfully supported the formation and growth of human colorectal cancer spheroids up to 44 days of culture. The spheroid dimension and density were influenced by the semi-IPN stiffness and permeability. These encouraging results would allow the implementation of faithful tumor models for the study and development of personalized oncological treatments.

1. Introduction

In vitro tumor models represent an important tool to study tumor complexity and validate drugs or combinations of drugs, towards the development of patient-specific treatments (Fang & Eglen, 2017). However, current experimental models in cancer research often fail to reproduce the heterogeneity of tumors and their complexity (Kamb, 2005; Zanoni et al., 2020). 2D cell culture systems do not allow faithful reproduction of cell physiology (Baker & Chen, 2012) and often distort the cellular behavior. As a consequence, they represent a poorly predictive drug testing model (Edmondson et al., 2014; Skardal et al., 2015). Contrarily, animal models can reproduce a higher level of complexity, but experimental costs, ethical concerns and species variability often prevent the extension of potential therapies to humans (Reidy et al., 2021). In order to bridge the gap between 2D *in vitro* cultures and animal models, organoids and spheroids are currently among the most promising tools for mimicking the complexity of human cancer in a 3D environment (Lau et al., 2020; Zanoni et al., 2020).

A simplified *in vitro* mimesis of the tumor structure is represented by multicellular spheroid cultures, obtained exploiting the ability of the tumor epithelial component to proliferate and self-assemble either on a non-adherent surface or immersed in a 3D matrix (Thakuri et al., 2018). From a morphological point of view, they recapitulate cell-cell, cell-matrix interaction, cell exposure to growth factors, conditions of hypoxia and acidic environment (Friedl & Wolf, 2003; Paschos et al., 2009). They are widely used in tumor biology research, allowing the study of tumor growth, angiogenesis, invasiveness and resistance to therapy (Thakuri et al., 2018). However, their drawbacks are the small size, limited by the supply of nutrients and oxygen to the inner cells (Achilli et al., 2012) and the large use of tumor cell lines (Thakuri et al., 2018).

Both biological and synthetic biomaterials have been proposed to support the formation and growth of several types of cells and spheroids, as extracellular matrix (ECM)-like analogues, driving a variety of cellular processes (Kamatar et al., 2020; Quarta et al., 2021). Chemically defined synthetic polymers have been largely used to develop hydrogels systems for 3D culture (Aisenbrey & Murphy, 2020). In contrast to

* Corresponding authors.
E-mail addresses: alessandro.polini@nanotec.cnr.it (A. Polini), francesca.gervaso@nanotec.cnr.it (F. Gervaso).
[1] These authors contributed equally to this study as senior authors.

https://doi.org/10.1016/j.carbpol.2021.118633
Received 18 June 2021; Received in revised form 30 August 2021; Accepted 31 August 2021
Available online 9 September 2021

synthetic polymers, which are considered biologically inert materials, natural hydrogels are ideal candidates for cell culture because of the presence of components similar to the ECM composition (Wieringa et al., 2018). Natural polymers (*e.g.* polysaccharides, proteins and animal derivatives) are able to bind water molecules and possess biodegradability and physicochemical properties including architecture, rigidity and porosity that can closely mimic the hydrated ECM of a tissue. Some natural hydrogels, thanks to the presence of matrix proteins, can be remodeled by cells and promote cell adhesion (Wieringa et al., 2018), although the poor stability of natural ECM-derived matrices often prevents their use in long-term culture (Blondel & Lutolf, 2019). Generally, organoid culture is associated with the use of animal ECM-materials such as matrigel and its derivatives (Blondel & Lutolf, 2019). However, the variability of mechanical and biochemical characteristics between different batches and within the same batch, and the antigenicity potential, related to the presence of animal-derived contaminants, make matrigel unsuitable for a reproducible representation of the cellular microenvironment, while its rapid degradability prevents its use in long-term culture studies, limiting its applicability to cell biology (Czerwinski & Spence, 2017). Natural and synthetic chemicophysically defined hydrogels are therefore widely proposed for organoid cultures, promoting cell expansion, differentiation and organization. For example, hybrid hydrogels, in which two or more biopolymers interact synergistically, offer the possibility to cover a higher range of physicochemical properties (Liu et al., 2019). The incorporation of a second network into a single polymeric hydrogel allows the development of interpenetrating polymer network (IPN) hydrogels with improved mechanical properties and the study of complex cell-matrix interactions (Dhand et al., 2020). Among natural polymers, polysaccharides, such as pectin, a linear, non-toxic, anionic plant polysaccharide characterized by the presence of galacturonic acid molecules, and chitosan, a deacetylated derivative of chitin, a cationic polysaccharide, localized in the exoskeleton of crustaceans, have been evaluated (Tentor et al., 2017). The combination of these two polymers can lead to the formation of physical hydrogels with the development of an interpolymer complex network (Nordby et al., 2003), occurring in an aqueous environment as a result of the electrostatic interaction between the positive amino groups of chitosan and the negative carboxyl groups of pectin under certain pH conditions (da Costa et al., 2016).

Here, we focused on the development of a composite biopolymer network for cell-encapsulation as 3D *in vitro* model, showing that chitosan and pectin can be successfully processed at mild conditions to obtain a thermo-sensitive hydrogel, suitable for cell-embedding and supporting the formation and growth of tumor spheroids. We exploited the salt-mediated ability of chitosan to gel at 37 °C while incorporating pectin into the system, leading to a semi-interpenetrating polymer network (semi-IPN). Generally, chitosan is soluble only at acidic pH and the neutralization of its positive charges through strong bases normally results in chitosan fiber precipitation. However, by using a weak base such as beta-glycerophosphate (βGP), it is possible to keep the deacetylated chitosan chains in solution at room temperature (r.t.) and physiological pH and induce the gel transition by increasing temperature, obtaining a thermo-sensible gel (A. Chenite et al., 2001). Here, we hypothesized that pectin can be introduced into the system, without losing the cell-embedding requirements but improving the system features with respect of the single-polymer hydrogel, and the use of such composite system to support the formation and growth of tumor spheroids as 3D models for colorectal cancer (CRC), which is the second leading cause of death in developed countries (Siegel et al., 2020). The extracellular environment in CRC is dynamic, constantly changing and plays an important role in tumor progression (Li et al., 2020). For this reason, it is important to develop an ECM-based model exhibiting the same degree of stiffness of the tumor microenvironment *in vivo* (Reidy et al., 2021). Hence, a further hypothesis of this study was that (*i*) the physicochemical properties of the chitosan-pectin composite can be tuned by varying the overall polymer concentration (Ch-Pec), but keeping constant the molarity of the βGP salt, and (*ii*) different systems with modulated degree of stiffness significantly affect the formation and extended culture (up to 44 days) of CRC spheroids *in vitro*.

2. Experimental section

2.1. Preparation of thermo-responsive hybrid hydrogels in chitosan-pectin

Low molecular weight chitosan (M_w 50 k–190 k Da based on viscosity, degree of deacetylation ≥75%; #448869 Sigma Aldrich, Milan, Italy) (Ch), Pectin from citrus peel (Galacturonic acid ≥74.0% dried basis, methoxy groups ≥6.7%, unknown M_w, #P9135 Sigma Aldrich) (Pec) and beta-glycerophosphate (βGP) (Sigma Aldrich) were used for hydrogel preparation. The hydrogels were obtained by solubilizing Ch powder (w/v) in aqueous solution of hydrochloric acid (HCl) 0.1 M and Pec powder (w/v) in deionized water (DI) under stirring at r.t. overnight. The Ch solution was further centrifuged at 1500 rpm for 5 min at 4 °C to remove bubbles. The two solutions were mixed in an optimized weight ratio (50:50) and centrifuged at 1500 rpm for 5 min at 4 °C. The gelling agent (βGP) was added to the resulting mix to induce a sol-gel transition at physiological temperature. The final total polymer concentration for High, Medium and Low hydrogels was 2.77%, 1.66% and 1%, respectively (details reported as Supplementary materials), keeping the molarity of βGP salt constant at 0.04 M. For some tests, 500 μL of complete DMEM was added to the final gel solution by the drop by drop technique and mixed through a spatula, in order to simulate the cell encapsulation step.

2.2. pH measurement, injectability and inversion tube test

The pH of the solutions of Ch, Pec, βGP, Ch-Pec mix and the final hydrogels was measured by test strips and monitored during the gelation process. Injection tests were performed by visual inspection, injecting all the hydrogel samples through a syringe connected to a 23G needle. In order to evaluate the thermo-sensitive sol-gel transition through the inversion tube test, the solutions were placed in vials at r.t. and 37 °C (physiological condition) and the fluidity/viscosity of the hydrogels was visually assessed through the inversion of the vial, at different experimental time points.

2.3. Rheological test

In order to determine the thermo-sensitivity of gelation process, rheological measurements were performed with an Anton Paar instrument (Physica MCR 301, Ostfildern, Germany) equipped with a two plates geometry (plate diameter 25 mm, gap distance 0.5 mm) and connected to a circulating water bath. Immediately following the High, Medium and Low hydrogels preparation, the variation of storage modulus (G′) and loss modulus (G″) with temperature was measured in the linear viscoelastic range, at constant shear strain (5%), constant frequency (1 Hz), while the temperature was increased from 7 to 42 °C at a rate of 1 °C/min. Each test was performed in duplicate.

2.4. Swelling test

The swelling ability of the hydrogels was assessed through gravimetric measurements, *i.e.* evaluating the weight variations of the hydrogel samples over time. Briefly, after thermal gelation (2 h at 37 °C), the samples were frozen at −20 °C, lyophilized overnight (LIO 5P, Cinquepascal, Milan, Italy) and weighed. The samples were immersed in phosphate-buffered saline (PBS) at 37 °C and weighed again at different time points. The swelling ratio percentage (SR) was calculated according to the following formula (1), where W_{dry} is the initial dry weight of the hydrogel and W_{wet} is the weight of the hydrogel after hydration in PBS and incubation at 37 °C:

$$SR\ (\%) = \left[\left(W_{wet} - W_{dry}\right)/W_{dry}\right] \times 100 \quad (1)$$

2.5. In vitro stability

The non-enzymatic degradation of the hydrogel over time was evaluated through the stability test. After gel formation, the samples were hydrated in PBS and incubated at 37 °C in oven, monitoring the weight at different time points. The percentage of weight loss (WL) was calculated according to the following formula (2), where W_0 is the initial weight of the hydrogel at $t = 0$ after thermal gelation and W_i is the weight of the hydrogel at different time points:

$$WL\ (\%) = [(W_0 - W_i)/W_0] \times 100 \quad (2)$$

2.6. Compression test

After thermal gelation, hydrogel samples were measured in terms of diameter and thickness and sandwiched between two impermeable and non-lubricated compression plates. Compression tests were performed in "wet" conditions at r.t. using a universal uniaxial machine (Zwicki-Line 1kN, Zwick Roell, Kennesaw, GA, USA) (Fig. S1). The average Young's modulus (E) was calculated as the slope of the linear part of the stress-strain curves at low strain values (0–5%) for each −DMEM formulation and +DMEM formulation with HCT-116 cell encapsulation at different time points.

2.7. Morphological analysis: image analysis and porosity measurement

The porous structure of the hydrogels, with and without the addition of DMEM solution during preparation, was observed by optical microscopy. After thermal gelation, the samples were frozen for 2 h at −20 °C and freeze-dried overnight. The samples were sectioned both longitudinally and transversely (L and T sections) and the sections were observed at different magnifications (5×–10×–20×). Finally, the measurement of the pore diameter of hydrogel formulations (High, Medium, Low) with and without the addition of DMEM was analyzed using ImageJ software (ImageJ bundled with 64-bit Java 1.8.0_172). Briefly, five microscopy images of different sections at magnification 5× were analyzed for each hydrogel typology after lyophilization, measuring the diameter as an average of two measurements for each pore, with a total of approximately 250 pores per sample.

2.8. Permeability test

The permeability to small proteins, nutrients and metabolites, was evaluated through the use of three fluorescein isothiocyanate−dextran molecules (FD, Sigma-Aldrich) having a Mw of 3 kDa–5 kDa (FD4), 20 kDa (FD20) and 59 kDa–77 kDa (FD70). Once the hydrogel solutions were prepared, 500 μL were placed into each vial and thermally gelified. Finally, 1 mL of labeled-dextran solution (1 mg/mL in PBS) was added on the surface of the hydrogel. After incubation at 37 °C, the FD concentration in the supernatant was quantified through absorbance at defined time points (1, 6 and 24 h), using a spectrophotometer (Varian Cary 50 UV–Vis, Agilent, Santa Clara, CA, US) at a wavelength of 490 nm and known and scalar concentrations of FD solutions as reference. Starting from formula (3), where C_i is the initial concentration of FD (1 mg/mL), V_i the initial volume of PBS (1 mL) and V_f the final volume of gel (0.5 mL) + FD (1 mL), it was possible to calculate the equilibrium concentration of FD, *i.e.* the maximum limit of dextran that can cross the gel, as well as the ratio between the final volume and the initial concentration of dextran in the solution. The equilibrium concentration was equal to 0.66 mg/mL:

$$C_f\ (mg/mL) = \left[(C_i \times V_i)/V_f\right] \quad (3)$$

2.9. Cell culture

Colorectal carcinoma cells (HCT 116, ATCC CCL-247, LGC Standards, Milan, Italy) were cultured in DMEM with 4.5 g/L glucose and sodium pyruvate without L-glutamine (Corning, Glendale, AZ, US), supplemented with 2 mM L-glutamine (Gibco), 10% Fetal Bovine Serum (FBS) (Corning), 100 U mL^{-1} penicillin and 100 μg mL^{-1} streptomycin (Gibco). Cells were incubated at 37 °C with 95% of humidity and 5% of carbon dioxide. 0.05% Trypsin-EDTA 1× (Corning) was used regularly to pass cells every 2–3 days preventing full confluence.

2.10. Cell encapsulation with HCT 116 within hydrogel formulations with different stiffness

After assessing the hydrogel biocompatibility and setting the optimal encapsulation cell density equal to 50,000 cells/mL of hydrogel, HCT 116 cells were encapsulated in hydrogel formulations with different stiffness (High, Medium, Low) and the formation of spheroids was monitored up to 44 days by optical microscopy (EVOS XL, Thermo Fisher Scientific, Waltham, MA, US). Another set of experiments was performed to compare the spheroid growth in the Medium formulation with single polymer control samples (2% Ch and 2% Pec).

Ch, Pec, βGP solutions were sterilized with UV light for 1 h, as well as everything needed for the cell encapsulation experiment, performed under a cell culture hood. Once the three different formulations of Ch-Pec-βGP 0.04 M hydrogel were prepared, 500 μL of DMEM containing the HCT-116 cells were added using the drop by drop technique and mixed gently with a spatula to evenly distribute the cells. Hydrogel spots (1 mL) were distributed in each well of a 24-well cell culture plate (6 aliquots for type of hydrogel) and incubated at 37 °C for 20 min to allow an initial gelation of the samples. Afterwards, each well containing gel was covered with 1 mL of DMEM for removing the salt residues, and replaced with complete DMEM after 10 min. The culture medium was replaced with fresh medium every 3 days.

Image analysis of spheroid formation and growth was performed using ImageJ software. Briefly, 40 microscopy images at magnification 20× were analyzed for each hydrogel type (High, Medium, Low) for different time points (0, 4, 10, 21, 30, and 44 days) to calculate the diameter and area of each spheroid. For the analysis of spheroids density, 5 images at lower magnification (4×) were analyzed for each hydrogel type at different time points (0, 4, 10, 30, 39, and 44 days).

2.11. Cell viability through live and dead staining

Cell viability of the HCT 116 spheroids in hydrogel was evaluated using a ReadyProbes Cell Viability Imaging Kit (Blue/Red) (Thermo Fisher). Briefly, 3 mL of DMEM with 6 drops of NucBlue Live Reagent and 6 drops of Propidium Iodide (PI) were prepared. Once the cell encapsulation was carried out, 1 mL of DMEM was removed from each well of a 6-well cell culture plate and 1 mL of DMEM with Live and Dead reagents was introduced. The samples were incubated for 2 h at 37 °C and cell viability was observed by fluorescence microscopy, with blue indicator for total cells and red for dead cells.

2.12. Analysis of CRC spheroids in hydrogel by DAPI/phalloidin staining

Spheroids grown in different hydrogel formulations were fixed at different time points (11, 21, 28 and 44 days). Briefly, an initial wash of the samples was performed with 1 mL PBS. 1 mL 4% paraformaldehyde was then added to each well. After 10–12 min at r.t., 3 washes in PBS were carried out to remove excess paraformaldehyde. For nucleic acid (DAPI) and cytoskeleton (phalloidin–TRITC) (Sigma-Aldrich) staining, 500 μL of (1:10,000 v/v) DAPI solution in PBS was added to each well and incubated at r.t. in the dark for 30 min. Afterwards, a washing step was carried out with 1 mL PBS and 400 μL of phalloidin solution (5 μg/mL) was added to each well, incubating for 1 h in the dark at r.t.. 2

washes with 1 mL PBS were carried out and finally 200 μL of PBS were added to cover the surface of the hydrogels.

2.13. Statistical analysis

All the experiments were performed in triplicate and the results are reported as the mean ± standard deviation. Data analysis and graphing were performed with Microsoft Excel 2019. Regarding the compression tests, GraphPad Prism software (v. 8.4.2) was employed to perform statistical analysis, using one-way ANOVA analysis.

3. Results

Thermo-sensitive hydrogel systems based on chitosan and pectin have been successfully developed exploiting the use of a wake base, namely βGP, as a thermal trigger for chitosan gelation (Assaad et al., 2015; Chenite et al., 2001; Zhou et al., 2015). A stable compound was formed in which pectin is incorporated and interpenetrated among chitosan chains, giving rise to a semi-IPN (Fig. 1). The first aim of this work was to design and develop a composite hydrogel in Ch-Pec able to overcome the limitations reported in literature regarding its preparation, such as high solubilization temperatures and use of highly acidic solutions.

Three different formulations were obtained (named High, Medium and Low) varying the Ch-Pec content and were subjected to deep analysis. The influence on the physicochemical properties of the small amount of cell culture medium (DMEM), needed to introduce the cells within the hydrogel, was evaluated comparing the obtained results with the hydrogel system without DMEM (named hereafter +DMEM and −DMEM).

3.1. pH measurement, injectability and inversion tube test

We measured the pH values of starting polymer and βGP solutions, as well as of final hydrogel (chitosan-pectin in 50:50 weight ratio, 0.04 M βGP) (Table S1). Despite the acidic pH values of the starting solutions, all the systems in Ch-Pec-βGP exhibited a pH range between 6 and 7 following the addition of the βGP and then reached a neutral pH value (pH = 7.4) immediately after mixing with DMEM, used to simulate cell encapsulation.

As reported in Table 1, all the hydrogel formulations were injectable at r.t., through a G23 needle (Videos S1–S3). The inversion tube test allowed evaluating the thermo-sensitive sol-gel transition by visually assessing the fluidity/viscosity of the hydrogels through the inversion of the vial, at both r.t. and 37 °C at different experimental time points. The higher polymer content formulation (High), due to the high viscosity, did not flow along the walls of the tube at r.t. (Fig. S2A). However, without increasing the temperature and incubating the sample for 2 h at 37 °C, a stable gel state could not be reached, demonstrating that thermal gelation did not occur. The intermediate formulation (Medium), characterized by lower viscosity, showed a slight and slow fluidity at r.t. However, after 2 h at 37 °C the sol-gel transition process resulted complete (Fig. S2B). On the contrary, the formulation with lower polymer concentration (Low) was able to flow at r.t., but also after 2 h of incubation at 37 °C, indicating that gelation process was not complete after 2 h (Fig. S2C). However, when the incubation at 37 °C was extended to 6 h, the fluidity drastically decreased (Videos S4 and S5).

Table 1
Overview of the results related to inversion tube test and injectability for different hydrogel formulations (High, Medium, Low).

Inversion tube test	High	Medium	Low
t = 0 r.t.	No flow	Flow	Flow
t = 2 h 37 °C	/	No flow	Flow (slow gelation)
t = 6 h 37 °C	/	/	Flow (slow gelation)
t = 24 h 37 °C	/	/	Flow (slow gelation)
Injectability at r.t.	Injectable	Injectable	Injectable

3.2. Rheological characterization of the thermo-sensitive gelation process

The temperature dependence of High, Medium and Low hydrogels storage modulus G′ is reported in Fig. 2. Upon heating from 5 to 50 °C, the temperature at which G′ rapidly increases gives an indication of the temperature of incipient gelation (Chenite et al., 2001). All three formulations show a thermo-sensitive behavior (Fig. S3) presenting an increase in the storage modulus G′ when temperature exceeds the 35 °C, while the loss modulus G″ remains almost constant in the 21–42 °C temperature range. As it can be observed in Fig. 2, the High and Medium formulations show significantly higher G′ values in comparison to the Low formulation.

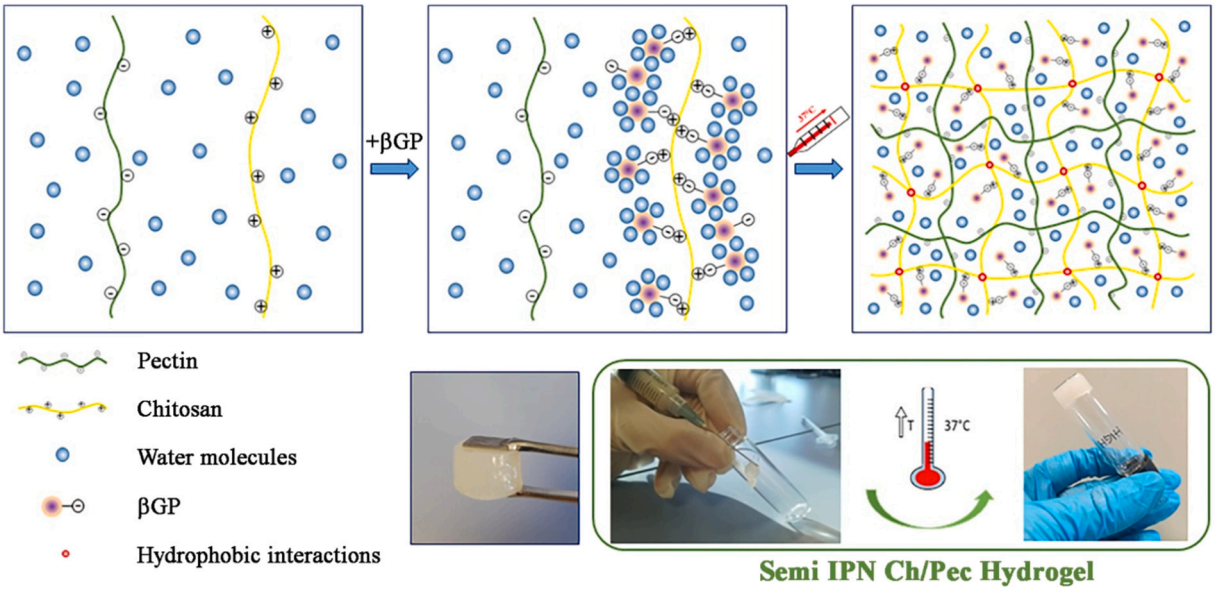

Fig. 1. Representation of Ch-Pec semi IPN development.

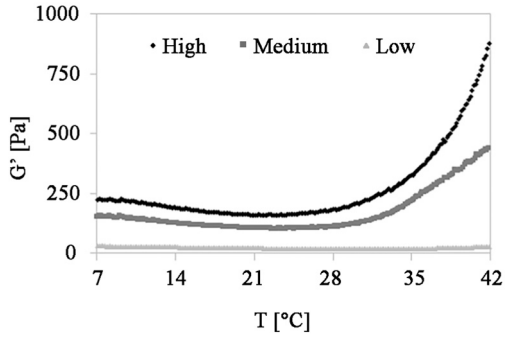

Fig. 2. Temperature-dependence of storage modulus G′ for High, Medium and Low hydrogels.

3.3. Swelling test and in vitro stability

The swelling test was conducted on hydrogels with and without addition of complete DMEM, up to 7 days of incubation at 37 °C. All the formulations showed a high swelling capacity already in the first 10 min of incubation in PBS at 37 °C; the High and Medium formulations showed a comparable trend, while the Low sample, with and without complete DMEM, showed a higher swelling ratio (>2000%) (Fig. 3A). Equilibrium was reached for all samples after a few hours and remained almost constant for up to 7 days (Fig. 3B).

The kinetics of hydrogel degradation was evaluated by stability test, conducted with or without DMEM addition, up to 49 days of incubation at 37 °C. All the formulations showed comparable degradation trends in the presence or absence of DMEM. The High samples were the most stable over time, compared to the Medium and Low formulations that, although showing different kinetics, completely degraded after 14 days at 37 °C (Fig. 3C–D).

3.4. Compression test

The compression test, aimed at evaluating the stiffness, *i.e.* Young's modulus, of the hydrogel systems (High, Medium, Low), allowed us to observe that there is a direct proportionality between the total polymer concentration and the hydrogel stiffness. No significant differences emerged between the formulations with or without DMEM. Significant differences were instead observed between the two more concentrated formulations (High and Medium) and the lower one (Low) (Fig. 4). No significant differences were observed between the Young modulus of High and Medium samples in the low strain range of (0–5%). However, significant differences were registered between the two specimens in the higher strain range, between 5 and 20%.

3.5. Morphological analysis: image analysis and porosity measurement

Optical microscopy was used to study the hydrogel structure (High, Medium and Low, all −DMEM and +DMEM). Image acquisition and morphological evaluation performed on freeze-dried samples sectioned longitudinally and transversely at different magnifications showed that all the formulations presented an open and highly interconnected porous structure (Figs. 5A–B, S4–S5). The image analysis allowed defining the pore diameter of the different formulations, whose average values ranged from 150 μm to 220 μm, with a comparable trend among the tested formulations. The High and Medium formulations showed larger pore size in the +DMEM formulation, while the Low sample showed a decrease in pore diameter in the −DMEM formulation (Fig. S6).

3.6. Permeability test

The diffusivity test carried out using fluorescent isothiocyanate-labeled dextran (FITC) at different molecular weights (MWs), *i.e.* 3–5 kDa, 20 kDa and 70 kDa, showed an inverse proportionality between MW and polymer concentration: the permeability to small proteins,

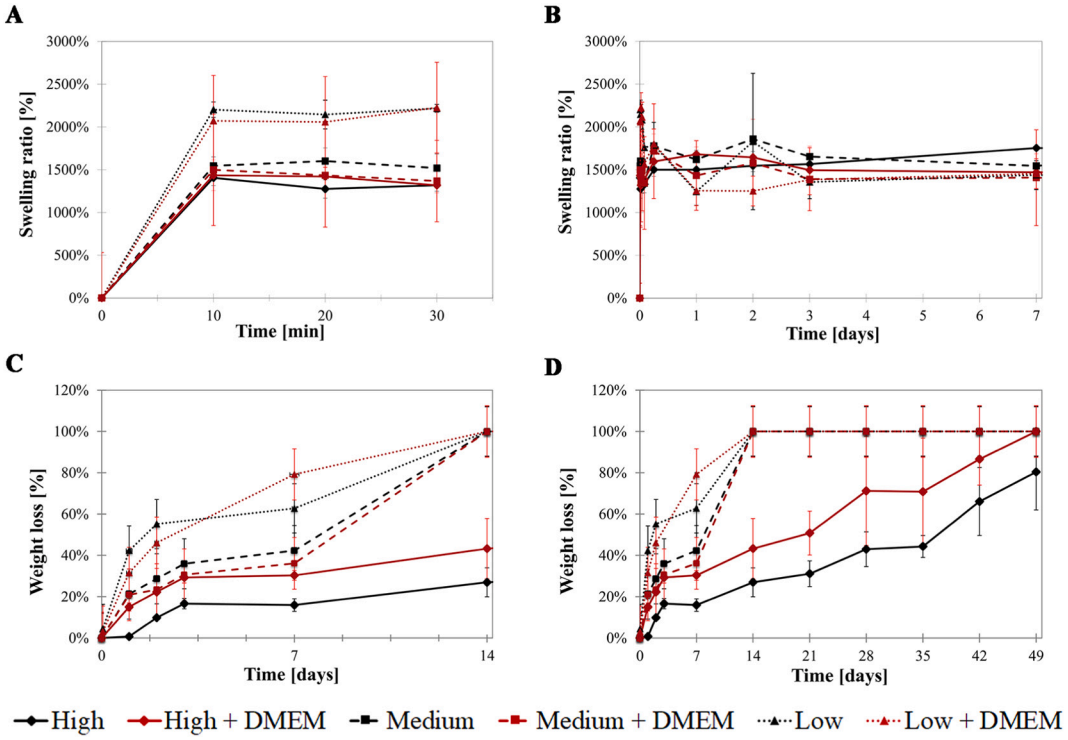

Fig. 3. Swelling test results for hydrogel formulations with and without DMEM addition, reported in a time frame of 30 min (A) and 7 days of incubation (B). Stability test results for hydrogel formulations with and without DMEM addition, reported in a time frame of 14 days (C) and 49 days of incubation (D).

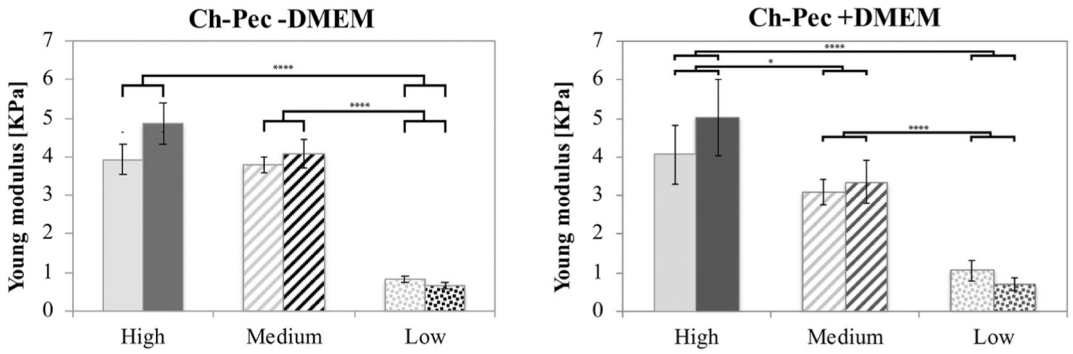

Fig. 4. Compression test results. Young's modulus calculated in two different strain range: 0–5% strain, (light colors) and 5–20% strain (dark colors) of High, Medium, Low hydrogel formulations both −DMEM (left) and +DMEM (right). *≤0.05, ****≤0.0001.

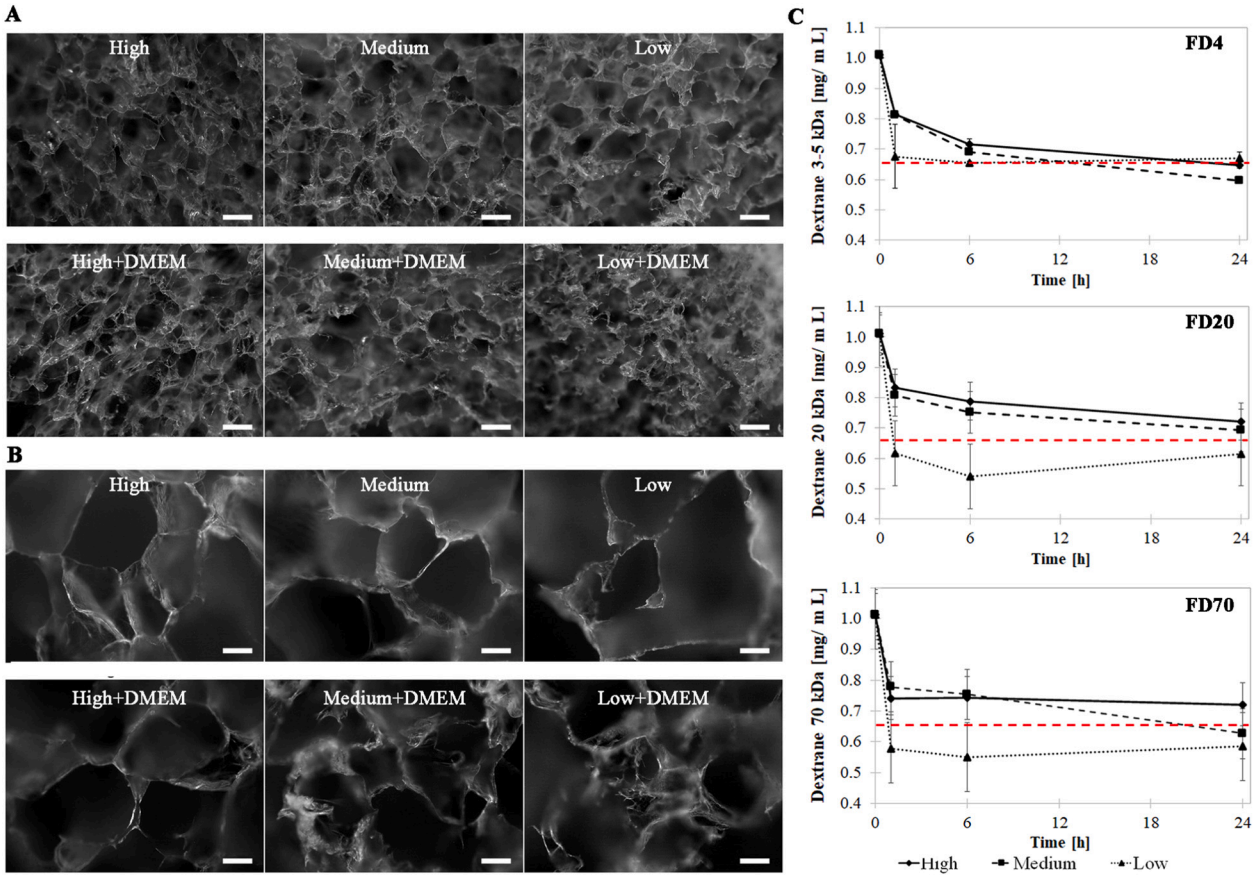

Fig. 5. Apparent porosity investigation and permeability tests. Morphological analysis of hydrogels with and without the addition of DMEM, at different magnification: 5× (A) (scale bar = 200 μm), 20× (B) (scale bar = 50 μm). Permeability test with FITC-dextran (FD) at different MW (FD4: 3 kDa–5 kDa; FD20: 20 kDa; FD70: 59 kDa–70 kDa) on different hydrogel formulations; the red dotted line represents the FD concentration at the equilibrium (C).

nutrients and metabolites was favored in the Low formulation which was the most permeable to the passage of dextran with different MWs, as shown in (Fig. 5C). In the plot relative to the lowest MW dextran, already in the first hour, the dextran concentration reached the equilibrium, *i.e.* the maximum concentration that could perfuse the hydrogel. In the other formulations, dextran needed longer time (24 h) to completely permeate the gel, achieving a permeability rate of 100% in all three samples. In addition, 20 kDa dextran easily diffused through the Low hydrogel, reaching a 100% diffusion rate in 24 h, and failed to completely diffuse through the more concentrated formulations (High and Medium) with a value of 83% and 91% at 24 h, respectively. On the other hand, 70 kDa dextran completely crosses the Low sample (100%) already in the first hour and the High and Medium formulations more slowly, with a value of 83% and 100% in 24 h.

3.7. Encapsulation of HCT 116 cells and growth of the spheroids in the three-hydrogel formulations

The immortalized human colorectal cancer cell line (HCT-116) was chosen to assay the ability of the three hydrogel formulations to promote the growth of 3D cellular structures and host the tumor spheroids for long-term studies. The cells were encapsulated within each type of hydrogel prior to the gel transition and the spheroids growth was monitored up to 44 days by optical microscopy observation and

statistically analyzed using image analysis software. Preliminary studies were carried out to set the optimal cellular density to be encapsulated: a concentration of 50,000 cells/mL was finally fixed to have a homogeneous cellular dispersion and a uniform distribution of the spheroids into the hydrogels minimizing the risk of generating fused spheroids from neighboring cells.

Size, morphology and density of the HCT 116 spheroids were affected by the stiffness and permeability of the hydrogel system (Fig. 6A). The formation of multicellular spheroids was observed in all chitosan-pectin hydrogels, and a prolonged viability (up to 44 days) was witnessed, although the initial spheroids growth rate was faster in the Medium and Low than in the High hydrogel formulation (Fig. 6). Indeed, the Medium and Low formulations already showed an active cell division process in the first 48 h, which led to the appearance of small spheroids (Fig. 6C) already after 4 days of culture, with an average diameter value of 49 μm and 43 μm, respectively. Instead, in the High formulation hydrogel, spheroids appeared with an average diameter value of about 58 μm, starting from day 10. Moreover, the morphology of spheroids grown in the High hydrogel formulations was irregular and, although some of them reached a large size (around 250 μm, Fig. 6C), the entire spheroids population was highly heterogeneous. On the other hand, spheroids grown in the Medium and Low formulations showed a lower but more homogeneous size (an average of 120 μm Fig. 5C) as well as a more regular morphology. These findings were confirmed by a statistical analysis performed to define both the average HCT 116 spheroids diameter and their area in the different hydrogel formulations (Figs. 6C, S7). The High samples showed a positive growing trend up to 30 days, while the other two reached a plateau value between the 10th and 20th day of culture. Analyzing the spheroid density, we found an inverse proportionality between stiffness and density: from a quantitative point of view, the Low sample presented a greater amount of spheroids, when compared with Medium and the High samples (Fig. 6B, D).

3.8. Effects of the spheroids growth on the hydrogels stiffness over time

Compression test was performed to evaluate the mechanical properties and therefore the degree of stiffness of the hydrogels at different time points of the *in vitro* culture, *i.e.* in the presence of HCT 116 cells or spheroids. The average Young's modulus (E) was then calculated at two

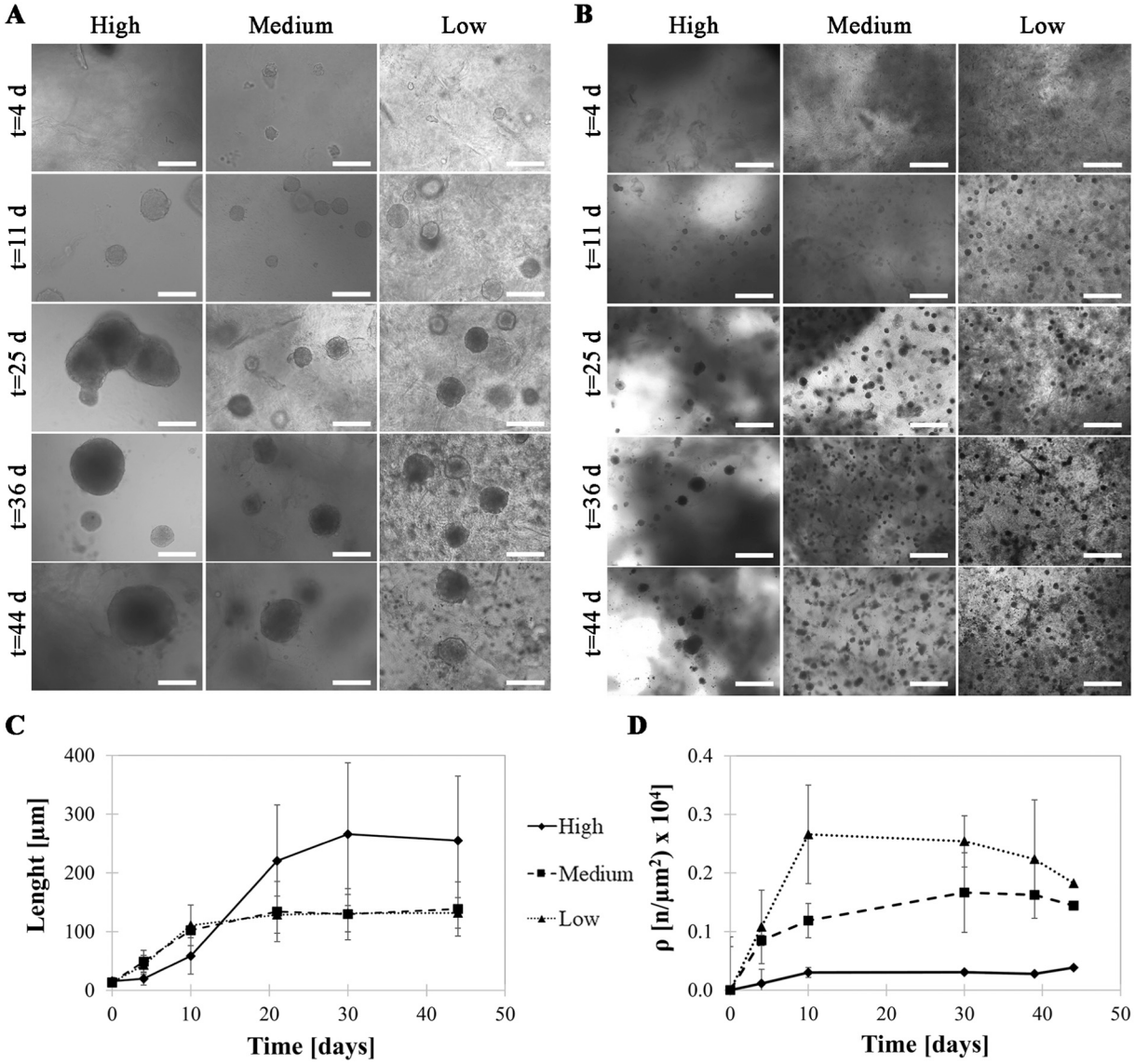

Fig. 6. Optical investigation and image analysis results of HTC 116 spheroid growth in Ch-Pec hydrogels. Morphological observation at different magnification of spheroid formation in High, Medium and Low hydrogel formulations up to 44 days of culture, scale bars: 200 μm (A) and 1000 μm (B). Plots of the average values (with standard deviation) of spheroid size (C) and density (D) at different time points.

strain ranges (0–5% and 5–20%) from the stress-strain curve obtained from compression test performed on the hydrogel formulations after HCT-116 cell encapsulation at different time points ($t = 0$, $t = 7$, $t = 14$, $t = 21$ days) (Fig. 7). The respective mean values and standard deviations have been plotted at each *in vitro* stage. The results showed that, in the first 2 weeks, the Young modulus at low strain values increased as the *in vitro* cell culture proceeded, while decreased at the third week of culture. A similar trend was observed for all the formulations, even if High and Medium hydrogels showed higher Young moduli than the Low one, as expected. In the 5–20% strain range, however, the slope of the stress-strain curve of both Medium and Low formulations did not show any significant changes related to the *in vitro* culture progression, while the High formulation Young modulus displayed a growing trend after 14 and 21 days.

3.9. Ch-Pec hydrogel synergistic effect in the formation of HCT 116 spheroids

In order to evaluate the effect of each polymeric component on spheroid growth, HCT 116 cells were encapsulated in either Ch-only or Pec-only hydrogels respectively. For the preparation of these hydrogels the molar amounts of Ch and Pec of the Medium formulation were used, since it proved to be optimal in terms of physicochemical properties. Pec-only hydrogels (in combination with βGP) were not able to sustain the growth of 3D structures (Figs. 8, S8) and, therefore, no spheroid formation was observed. On the other hand, chitosan with βGP (0.04 M) underwent the thermal sol-gel transition, achieving a 3D architecture. This led to the appearance of a few spheroids with an average diameter of about 150–200 μm, only after 2 weeks of culture. Noteworthy, the Ch-Pec formulation with βGP showed a higher number of spheroids over time than Ch-only. Therefore, these results highlighted the synergistic effect of chitosan-pectin mix, with respect to the Ch-only and Pec-only control solutions.

3.10. Comparative analysis of CRC spheroids grown in the three hydrogel formulations

The cell viability of HCT-116 spheroids was assessed using the Live and Dead Assay, performed at different experimental time points from day 7 to day 44 of culture (Fig. 9A). Spheroids exhibited high viability (represented by blue color) in all the tested formulations until day 21. Starting from day 28 of culture, a necrotic core (red area in the image) appeared evident in all the samples. Spheroidal growth was optimally supported by the developed hydrogel systems, as shown by DAPI/Ph staining at day 28 (Figs. 9B, C, S9–S11).

4. Discussion

3D culture systems based on the use of a supporting material such as hydrogels allow cells to experiment the typical three-dimensional architecture of *in vivo* organs and have become a valid tool for the study of tumor microenvironment and of the pathological mechanisms involved in tumor development. Here, we developed a natural composite hydrogel system in chitosan and pectin, featuring a thermo-responsive behavior, tunable mechanical properties, and high biocompatibility.

Chitosan and pectin matrices have been largely used in the fields of tissue engineering and *in vitro* models (Birch et al., 2015; Martins et al., 2018; Michailidou et al., 2021; Neves et al., 2015; Rangel, 2015; Stanzione et al., 2020; Tentor et al., 2017), as well as drug delivery (Cheikh et al., 2019; Long et al., 2019; Neufeld & Bianco-Peled, 2017; Torpol et al., 2019). However, Ch-Pec composite hydrogels have never been employed in cancer research, although we witnessed some attempts in chitosan-based 3D culture systems: *e.g.* micromolded photocrosslinkable chitosan hydrogels for hepatoblasoma (Hep G2) and fibroblast cells (NIH-3 T3) co-culture spheroids (Fukuda et al., 2006), and chitosan-PEG thermo-responsive hydrogels for liver cancer and glioma spheroids (Chang et al., 2018; Liu et al., 2015).

Chitosan and pectin powders, however, are often solubilized using acidic solutions and high temperatures (60 °C to 97 °C), conditions not compatible with cell culturing. Ch-Pec hydrogels are usually in the gel state at room temperature and in the liquid state at high temperature (Birch et al., 2015; Hiorth et al., 2005; Long et al., 2019; Martins et al., 2018; Neufeld & Bianco-Peled, 2017; Shitrit et al., 2019; Tentor et al., 2017; Torpol et al., 2019; Ventura & Bianco-Peled, 2015). In a recent study, a printable Ch-Pec hydrogel was developed by solubilizing the powder in acetic acid and reaching the temperature of 80 °C, to promote pectin solubilization and sol-gel transition at 50 °C (Michailidou et al., 2021). In the present work, the Ch-Pec semi-IPN exploits the βGP-mediated gelation method of chitosan, incorporating pectin into the network at the same time.

As extensively reported in literature(Chenite et al., 2001; Chenite et al., 2000; Supper et al., 2013; Zhou et al., 2015), the addition of βGP in an acidic chitosan solution will result in a neutral solution without chitosan fiber precipitation. The βGP/chitosan/water system is liquid at room temperature but starts the sol-gel transition when heated at 37 °C. In our work, we exploited the chitosan/βGP capacity to create a polymeric hydrogel network by increasing temperature to incorporate a second polymer, *i.e.* pectin. Thus, the system we proposed in our study comprises one network, chitosan/βGP physically "cross-linked" hydrogel, and one branched polymer, pectin, that are not covalently bonded to each other, but are at least partially interlaced on a molecular scale, originating a semi-IPN (Matricardi et al., 2013). This system proved to

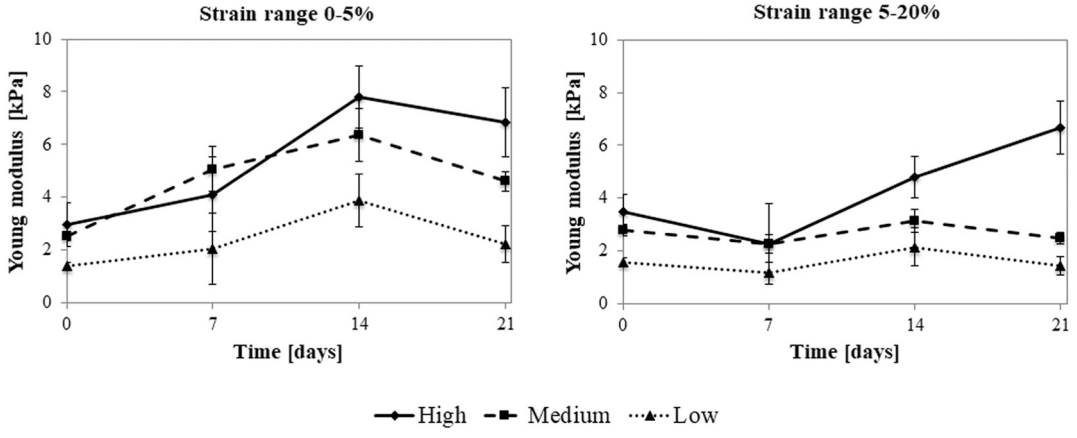

Fig. 7. Young modulus at different days of *in vitro* culture for the three hydrogel formulations (High, Medium, Low) at low (left) and high (right) strain range. The values are reported as mean ± standard deviation ($n = 5$).

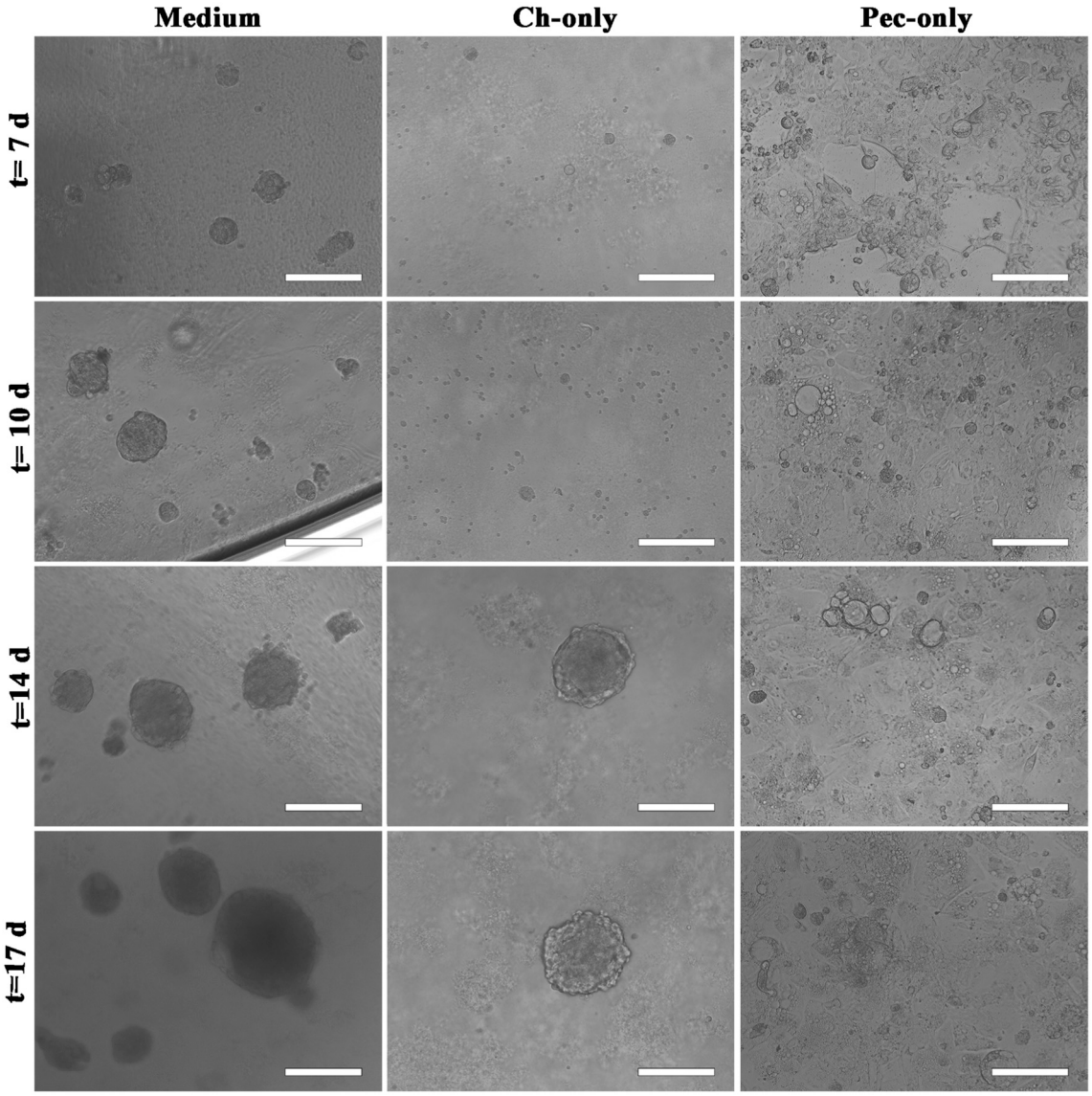

Fig. 8. Monitoring of HCT-116 spheroid growth in the Medium hydrogel formulation, compared to the Ch-only and Pec-only control samples (Scale bars: 200 μm).

be tunable and supported the *in vitro* culture of colorectal cancer spheroids. In order to modulate the physicochemical properties of the hydrogel, we varied the stiffness by modulating the concentration of final polymer in the gel; thus, we developed several formulations, which were subjected to physicochemical characterization. We selected three formulations with mechanical properties in the range of healthy colon tissue (Nebuloni et al., 2016). All the systems (High, Medium and Low) had a pH suitable for cell viability, were injectable at r.t., showing sol-gel transition at 37 °C and overcoming the limit of all reported studies on chitosan pectin systems in which high temperature and/or strong acidic conditions are used in the hydrogel preparation procedure, procedures not suitable for cell embedding. In terms of sol-gel transition, despite the viscosity of the system which reduced the fluidity at r.t. in the High and Medium formulations, incubation at 37 °C over time (from few minutes for small samples up to 2 h) was a necessary requirement for gelation to occur. The Low formulation, instead, showed a slower thermal gelation process (up to 6 h) probably because of the very low polymer concentration.

The stability test conducted on the different hydrogel formulations +DMEM and −DMEM up to 6 weeks of incubation at 37 °C highlighted that the High sample −DMEM was the most stable while the Low one showed the highest degradation rate, dissolving completely after 2 weeks in the absence of cells. Although a significant comparison between our degradation results and similar ones from literature cannot be performed because of the strong dissimilarity with other Ch-Pec systems, we can highlight that our High formulation is very stable (16% of weight loss in 1 week) and that the degradation rate and *in vitro* stability can be easily modulated varying the polymer concentration (Medium 42%, Low 63%). In another study (Bombaldi de Souza et al., 2020), the weight loss of Ch-Pec tubular scaffold was equal to 30.8% after 7 days of incubation at 37 °C in PBS. This value falls in the range between our High and Medium formulation weight loss.

In general, we found less degradation of the Ch-Pec matrices at different formulations in DMEM and this allowed us to conduct long-term culture. DMEM has a well-defined known composition and is a culture medium rich in ions, glucose, vitamins, proteins, amino acids and other nutrients that are essential for cell growth (Yao & Asayama, 2017). Among the constituents, amino acids in particular are characterized by the presence of an amine and carboxyl group and R group (side chain), which, based on their nature, allows them to be classified into polar, non-polar, aromatic and positively and negatively charged, depending on the pH of the solution (Lehninger et al., 2005). As reported in a recent paper by Yan and colleagues in 2019, amino acids can interact with different biomolecules in an aqueous solution by

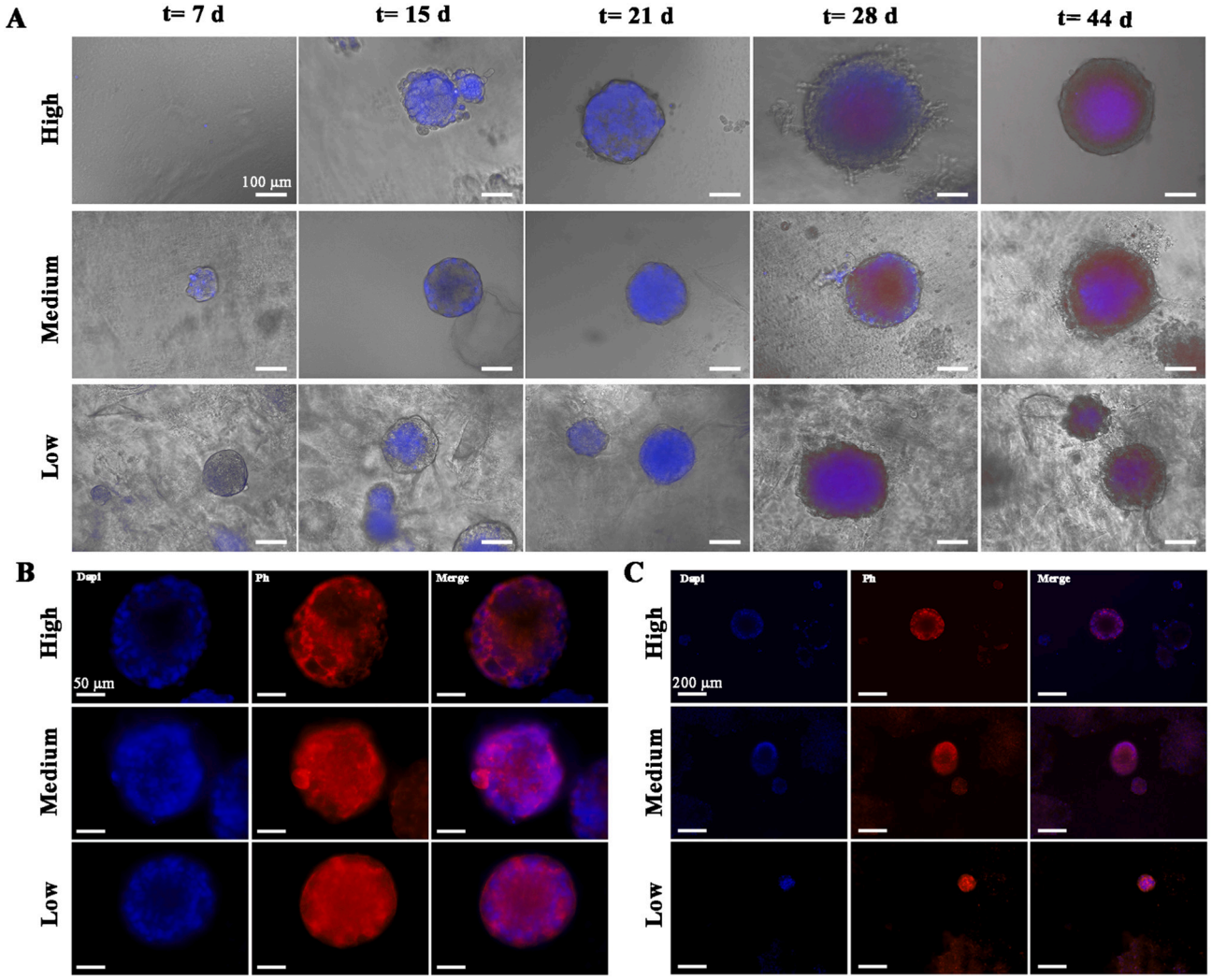

Fig. 9. Viability assessment of HTC 116 spheroids in Ch-Pec hydrogels. Live and Dead Assay test at different time points (blue: total cells; red: dead) (A); DAPI/Ph staining after 28 days of HCT 116 spheroid culture (blue: DAPI; red: Ph *F-actin*) at different magnification: 40× (B) and 10× (C). (For interpretation of the references to color in this figure legend, the reader is referred to the web version of this article.)

hydrophilic and hydrophobic molecular interactions (Yan et al., 2019), generally leading to a more compact structure of the molecules dissolved in solution (Jamal et al., 2014). In our study, the reduced degradation kinetics of Medium and Low samples visually observed in DMEM, might be ascribed to the phenomenon just mentioned, allowing the matrices to become more stable in the presence of DMEM and support long-term cultures of CRC spheroids. This hypothesis should be better investigated in the future.

The swelling tests showed that, reaching the maximum swelling ratio (about 1500–2000%) within 10 min, the different composite hydrogels were able to swell faster and at a higher degree in comparison to other Ch-Pec systems reported in literature. In another study, Ch-Pec hydrogels, despite a rapid swelling (in about 15 min), reached a swelling ratio value of 370% (Birch et al., 2015), while another system showed a swelling value of 150–200% in about 1 h, thus significantly lower and in a longer time than our formulations (Bernabé et al., 2005). Other studies reported even longer times to reach maximum swelling (Michailidou et al., 2021; Neufeld & Bianco-Peled, 2017; Shitrit et al., 2019; Sigaeva et al., 2020). Swelling ratio values similar to our systems are rarely found in Ch-Pec hydrogels: *e.g.* a value of 2832% was reported, although the equilibrium was reached after 2 h (Long et al., 2019). In a recent study, Ch-Pec hydrogels showed a swelling ratio value over 800% and reached the equilibrium at day 10, when hydrolytic degradation began (Ghorbani et al., 2020).

By optical investigation, we analyzed the hydrogel structure and noticed an open and highly interconnected pore structure in all the systems, similarly to Ch-Pec hydrogels with cellulose nanocrystals (Ghorbani et al., 2020). The High and Medium formulations presented a slightly higher pore size porous structure, compared to the Low formulation, probably because of the weak structure of Low samples that partially collapsed. However, from a careful statistical analysis of the results (Fig. S6), there are no significant differences among the different formulations and, therefore, the porosity was not affected by the percentage of final polymer used in our study, showing mean values in the range of 150–220 µm. This is lower than most Ch-Pec hydrogels (often higher than 350 µm) (Bombaldi de Souza et al., 2020; Tentor et al., 2017), although lower values (from 15 µm to 110 µm) were observed in some Ch-Pec or Ch-only hydrogels (Birch et al., 2015; Boido et al., 2019). Taking into account their swelling ability, with the High and Medium samples swelling less in the first 10 min and being more stable over time compared to the Low formulation, this is likely due to a tightly cross-linked structure and, therefore, to the presence of more compact pores. On the contrary, Low samples, visually showing a loose porous structure, had a higher swelling ratio % but degraded more quickly. However, we would like to point out that the freezing process might modify the hydrogel structure due to ice crystal solid state phase

separation artifacts. Although an overestimation of the pore size might occur with this process, we believe that the observed porosity is related to the original hydrogel structure and the results should not be considered as "absolute" values but relative one each other.

A hydrogel system developed for 3D cell culture systems must be permeable to the passage of small and medium-sized molecules as well as gases, *e.g.* nutrients and waste substances of cellular metabolism. Our tests, performed using FITC-labeled dextran (FD) at different MW as test molecule, showed a good hydrogel permeability, and an inverse proportionality between the permeability and the concentration of final polymer. In previous studies on Ch-βGP thermo-responsive hydrogels (Boido et al., 2019), uptake kinetics were strongly affected by FD MW, showing that after 24 h of incubation 70% and 40% of FD4 and FD20, respectively, were absorbed. These data are far from our results: after 24 h, FD4 was completely diffused into the hydrogel in all the formulations, while FD20 diffused for 83%, 91% and 113%, respectively in High, Medium and Low hydrogel formulations. Sahu and colleagues observed that the percentage of dextran passing through graphene oxide-Pluronic thermo-responsive gel was affected by the gel mechanical properties, and higher elastic modulus was associated with slower release of labeled dextran (Sahu et al., 2012). The release rate of FD70 reached a maximum of 40% after 24 h, while in our study it completely crossed the Medium and Low formulations and reached 80% in the High formulation. This is likely due to the different hydrogel composition under evaluation.

During different stages of organoid culture development, mechanical properties play a crucial role (Blondel & Lutolf, 2019). The fundamental processes of growth, differentiation, and expansion are, indeed, strongly affected by matrix stiffness, and there is currently large interest on the use of mechanically defined matrices (Liu et al., 2019). Precisely controlled matrices for 3D tumor cultures can lead to a greater understanding of the cancer cell phenotype, cell-ECM interaction, and response to drug treatment. For example, in a recent work by Dominijanni and colleagues, collagen matrix remodeling, in the presence of a stromal component, influenced the malignant phenotype of tumor cells and their proliferative power. Specifically, an increase in the matrix mechanical properties (Young's modulus value from 10 kPa to 30 kPa) inhibited cell growth and reduced the response to chemotherapy (Dominijanni et al., 2020). Here, the compression test was used to evaluate the mechanical properties of hydrogels. We found a direct proportionality between hydrogel stiffness and polymer concentration, with relatively low Young's modulus (E) (1–4 kPa), in close agreement with the behavior and values reported for chitosan hydrogels (0.5–1.5 kPa) (Shitrit et al., 2019) and Ch-Pec scaffolds (2 kPa) (Bombaldi de Souza et al., 2020), and comparable to those of the ECM of healthy biological tissues (0.1–1 kPa) (Wang et al., 2014). Furthermore, there were no significant differences between the −DMEM and +DMEM hydrogel, indicating that the amount of DMEM introduced into the system to deliver cells inside the system, is small enough to do not induce any change in the hydrogel mechanical properties. The values are in agreement with the Young's modulus values recorded for healthy colon tissue, between 2 and 5 kPa, in contrast to the stiffness of CRC tumor tissue, which instead reaches higher values, between 15 and 40 kPa (Nebuloni et al., 2016).

Compression tests were also performed to follow up the variation of the mechanical properties and, therefore, the degree of stiffness, as the spheroids grow into the hydrogels over time (up to 21 days). The results showed that the hydrogel stiffness at very low strain values (0–5%) increased for all the formulations in the first two weeks of culture, then decreased at the third week. The mechanical data suggest that in the first 14 days the processes of spheroids formation and cell-mediated ECM synthesis are predominant on the hydrogel degradation process. At 21 days, the trend reversed hinting that the Ch-Pec matrix started to degrade more significantly, as confirmed by the hydrogel weight loss data from the stability test.

Once the different hydrogel formulations were tested in 3D cell culture studies, we observed an excellent ability to support the formation of spheroids and growth up to 44 days of culture, with the most concentrated formulation characterized by a high heterogeneity in spheroid size when compared to the intermediate and soft formulations. Generally speaking, we noted a high viability of HCT-116 cells up to day 21 and appearance of the characteristic necrotic core at day 28. This appearance is a typical feature of 3D cancer models. Generally, spheroidal systems present a spatially well-defined cellular organization, with an outer zone of proliferative cells, an intermediate region of quiescence and senescence, and an apoptotic cell zone in the core (Zanoni et al., 2020).

Currently, no work related to the development of tumor spheroids in Ch-Pec-based hydrogels is reported in the literature, while other systems were employed for the formation of 3D colorectal cancer systems. The immortalized colon cancer cell line HCT-116 was used, for example, to form organoids of HCT-116 and hepatocytes in collagen I hydrogels and hyaluronic acid microcarriers, maintained in culture for 14 days (Devarasetty et al., 2017). The same cell line was used in PEG diacrylate, gelatin, and hyaluronic acid hydrogels to develop colorectal organoids, maintained for 14 days (Forsythe et al., 2020). From the Live and Dead test, no appearance of necrotic core was observed at day 14 of culture, in agreement with our system. An injectable hyaluronic acid-cyclodextrins hydrogel was able to support the formation of HCT-116 spheroids and their growth for up to 21 days, reaching a diameter of 342 μm (Fiorica et al., 2020). HCT-116 spheroids were also formed without the use of hydrogels, but employing ultra-low attachment cell plates (Tchoryk et al., 2019). The spheroids were maintained in culture for 14 days, reaching a diameter of approximately 430 μm, in contrast to the diameter range of 200–250 μm found in our study. Recently, a hydrogel based on methylcellulose and hyaluronic acid facilitated the formation of HCT-116 spheroids, with a maximum spheroid growth of 320 μm at 7 days of culture (Mahboubian et al., 2020). These findings are comparable with our results, particularly with the High formulation, in which an exponential growth of spheroids was observed up to day 30 of culture, with sizes from day 10 to day 21 being 83 μm and 219 μm, respectively. In agreement with this study, we observed the formation of spheroidal aggregates at 7 days, but the authors noticed the appearance of a necrotic core already at day 7 of culture. In our formulations, the necrotic core appeared only from day 28 of culture, demonstrating that our hydrogels presented a structure with a certain combination of stiffness, permeability and porosity, which allows the transport of oxygen and nutrients up to the center of the spheroid for longer culture times.

Although our findings confirm the suitability of these thermo-responsive composite hydrogels for the development of 3D CRC *in vitro* models, the present study has some limitations. First, a simplified, monoculture-derived model has been proposed, while highly pathologically-relevant tumor tissue models should involve several cell types in order to mimic, among the others, relevant phenomena, such as immunological responses and vascularization. Future investigations have been planned to increase the complexity of our system, by focusing on co-culture studies (HCT-116 cells with cancer associated fibroblasts and mast cells). Second, an in-depth analysis of the relationship between the hydrogel stiffness and tumor spheroid development could also consider the intracellular pathway related to mechanotransduction, *e.g.* by assessing the Hippo pathway effectors (YAP/TAZ). This would shed the light towards a better understanding of tumor spheroid formation *in vitro*.

5. Conclusions

To summarize, in this work a thermo-responsive composite hydrogel was developed, characterized by the optimal combination of two natural polymers such as chitosan and pectin, able to interconnect homogeneously and generate a semi-IPN, supporting the formation of large spheroids of CRC cells for up to 44 days of culture. Furthermore, the

system showed tunable mechanical properties, with Young's modulus values comparable to ECM stiffness of biological tissues. The developed hydrogel formulations showed a variable degree of stiffness in relation to the different concentration of total final polymer used and, in turn, they led to different growth behaviors of colorectal spheroids, in terms of density and dimensions. These thermo-responsive hybrid hydrogels will be helpful in the standardization of *in vitro* culture of 3D tumor models for patient-specific studies of drug-response and tumor progression.

Additional experimental section; additional figures and videos regarding pH measurement, injectability and inversion tube test, morphological analysis, permeability test, cell encapsulation studies and mechanical characterization. Supplementary data to this article can be found online at https://doi.org/10.1016/j.carbpol.2021.118633.

CRediT authorship contribution statement

Giulia Morello: Methodology, Validation, Formal analysis, Writing – original draft, Writing – review & editing. **Alessandra Quarta:** Methodology, Formal analysis, Writing – review & editing. **Antonio Gaballo:** Methodology, Formal analysis, Writing – review & editing. **Lorenzo Moroni:** Writing – review & editing, Supervision. **Giuseppe Gigli:** Writing – review & editing, Supervision, Funding acquisition. **Alessandro Polini:** Conceptualization, Methodology, Writing – original draft, Writing – review & editing, Supervision. **Francesca Gervaso:** Conceptualization, Methodology, Formal analysis, Writing – review & editing, Supervision.

Acknowledgements

The authors are grateful to the “Tecnopolo per la medicina di precisione” (TecnoMed Puglia) - Regione Puglia: DGR n.2117 del 21/11/2018, CUP: B84I18000540002 and “Tecnopolo di Nanotecnologia e Fotonica per la medicina di precisione” (TECNOMED) - FISR/MIUR-CNR: delibera CIPE n.3449 del 7-08-2017, CUP: B83B17000010001.

References

Achilli, T. M., Meyer, J., & Morgan, J. R. (2012). Advances in the formation, use and understanding of multi-cellular spheroids. *Expert Opinion on Biological Therapy, 12*(10), 1347–1360. https://doi.org/10.1517/14712598.2012.707181

Aisenbrey, E. A., & Murphy, W. L. (2020). Synthetic alternatives to Matrigel. *Nature Reviews Materials, 5*(7), 539–551. https://doi.org/10.1038/s41578-020-0199-8

Assaad, E., Maire, M., & Lerouge, S. (2015). Injectable thermosensitive chitosan hydrogels with controlled gelation kinetics and enhanced mechanical resistance. *Carbohydrate Polymers, 130*, 87–96. https://doi.org/10.1016/j.carbpol.2015.04.063

Baker, B. M., & Chen, C. S. (2012). Deconstructing the third dimension: How 3D culture microenvironments alter cellular cues. *Journal of Cell Science, 125*(Pt 13), 3015–3024. https://doi.org/10.1242/jcs.079509

Bernabé, P., Peniche, C., & Argüelles-Monal, W. (2005). Swelling behavior of chitosan/pectin polyelectrolyte complex membranes. Effect of thermal cross-linking. *Polymer Bulletin, 55*(5), 367–375.

Birch, N. P., Barney, L. E., Pandres, E., Peyton, S. R., & Schiffman, J. D. (2015). Thermal-responsive behavior of a cell compatible chitosan/pectin hydrogel. *Biomacromolecules, 16*(6), 1837–1843. https://doi.org/10.1021/acs.biomac.5b00425

Blondel, D., & Lutolf, M. P. (2019). Bioinspired hydrogels for 3D organoid culture. *Chimia (Aarau), 73*(1), 81–85. https://doi.org/10.2533/chimia.2019.81

Boido, M., Ghibaudi, M., Gentile, P., Favaro, E., Fusaro, R., & Tonda-Turo, C. (2019). Chitosan-based hydrogel to support the paracrine activity of mesenchymal stem cells in spinal cord injury treatment. *Scientific Reports, 9*(1), 1–16.

Bombaldi de Souza, F. C., Camasão, D. B., Bombaldi de Souza, R. F., Drouin, B., Mantovani, D., & Moraes, Â. M. (2020). A simple and effective approach to produce tubular polysaccharide-based hydrogel scaffolds. *Journal of Applied Polymer Science, 137*(13), 48510.

Chang, F. C., Levengood, S. L., Cho, N., Chen, L., Wang, E., Yu, J. S., & Zhang, M. (2018). Crosslinked chitosan-PEG hydrogel for culture of human glioblastoma cell spheroids and drug screening. *Advanced Therapeutics, 1*(7), Article 1800058.

Cheikh, D., García-Villén, F., Majdoub, H., Zayani, M. B., & Viseras, C. (2019). Complex of chitosan pectin and clay as diclofenac carrier. *Applied Clay Science, 172*, 155–164.

Chenite, A., Buschmann, M., Wang, D., Chaput, C., & Kandani, N. (2001). Rheological characterisation of thermogelling chitosan/glycerol-phosphate solutions. *Carbohydrate Polymers, 46*(1), 39–47. https://doi.org/10.1016/S0144-8617(00)00281-2

Chenite, A., Chaput, C., Wang, D., Combes, C., Buschmann, M., Hoemann, C., … Selmani, A. (2000). Novel injectable neutral solutions of chitosan form biodegradable gels in situ. *Biomaterials, 21*(21), 2155–2161.

Czerwinski, M., & Spence, J. R. (2017). Hacking the matrix. *Cell Stem Cell, 20*(1), 9–10. https://doi.org/10.1016/j.stem.2016.12.010

da Costa, M. P. M., de Mello Ferreira, I. L., & de Macedo Cruz, M. T. (2016). New polyelectrolyte complex from pectin/chitosan and montmorillonite clay. *Carbohydrate Polymers, 146*, 123–130. https://doi.org/10.1016/j.carbpol.2016.03.025

Devarasetty, M., Wang, E., Soker, S., & Skardal, A. (2017). Mesenchymal stem cells support growth and organization of host-liver colorectal-tumor organoids and possibly resistance to chemotherapy. *Biofabrication, 9*(2), Article 021002.

Dhand, A. P., Galarraga, J. H., & Burdick, J. A. (2020). Enhancing biopolymer hydrogel functionality through interpenetrating networks. *Trends in Biotechnology*. https://doi.org/10.1016/j.tibtech.2020.08.007

Dominijanni, A., Devarasetty, M., & Soker, S. (2020). Manipulating the tumor microenvironment in tumor organoids induces phenotypic changes and chemoresistance. *iScience, 23*(12), Article 101851.

Edmondson, R., Broglie, J. J., Adcock, A. F., & Yang, L. (2014). Three-dimensional cell culture systems and their applications in drug discovery and cell-based biosensors. *Assay and Drug Development Technologies, 12*(4), 207–218. https://doi.org/10.1089/adt.2014.573

Fang, Y., & Eglen, R. M. (2017). Three-dimensional cell cultures in drug discovery and development. *SLAS Discovery, 22*(5), 456–472. https://doi.org/10.1177/1087057117696795

Fiorica, C., Palumbo, F. S., Pitarresi, G., Puleio, R., Condorelli, L., Collura, G., & Giammona, G. (2020). A hyaluronic acid/cyclodextrin based injectable hydrogel for local doxorubicin delivery to solid tumors. *International Journal of Pharmaceutics, 589*, Article 119879.

Forsythe, S., Mehta, N., Devarasetty, M., Sivakumar, H., Gmeiner, W., Soker, S., … Skardal, A. (2020). Development of a colorectal cancer 3D micro-tumor construct platform from cell lines and patient tumor biospecimens for standard-of-care and experimental drug screening. *Annals of Biomedical Engineering, 48*(3), 940–952.

Friedl, P., & Wolf, K. (2003). Tumour-cell invasion and migration: Diversity and escape mechanisms. *Nature Reviews. Cancer, 3*(5), 362–374. https://doi.org/10.1038/nrc1075

Fukuda, J., Khademhosseini, A., Yeo, Y., Yang, X., Yeh, J., Eng, G., … Langer, R. (2006). Micromolding of photocrosslinkable chitosan hydrogel for spheroid microarray and co-cultures. *Biomaterials, 27*(30), 5259–5267.

Ghorbani, M., Roshangar, L., & Rad, J. S. (2020). Development of reinforced chitosan/pectin scaffold by using the cellulose nanocrystals as nanofillers: An injectable hydrogel for tissue engineering. *European Polymer Journal, 130*, Article 109697.

Hiorth, M., Kjøniksen, A.-L., Knudsen, K. D., Sande, S. A., & Nyström, B. (2005). Structural and dynamical properties of aqueous mixtures of pectin and chitosan. *European Polymer Journal, 41*(8), 1718–1728. https://doi.org/10.1016/j.eurpolymj.2005.02.028

Jamal, M. A., Khosa, M. K., Rashad, M., Bukhari, I. H., & Naz, S. (2014). Studies on molecular interactions of some sweeteners in water by volumetric and ultrasonic velocity measurements at T=(20.0–45.0 C). *Food Chemistry, 146*, 460–465.

Kamatar, A., Gunay, G., & Acar, H. (2020). Natural and synthetic biomaterials for engineering multicellular tumor spheroids. *Polymers, 12*(11), 2506.

Kamb, A. (2005). What's wrong with our cancer models? *Nature Reviews. Drug Discovery, 4*(2), 161–165. https://doi.org/10.1038/nrd1635

Lau, H. C. H., Kranenburg, O., Xiao, H., & Yu, J. (2020). Organoid models of gastrointestinal cancers in basic and translational research. *Nature Reviews. Gastroenterology & Hepatology, 17*(4), 203–222. https://doi.org/10.1038/s41575-019-0255-2

Lehninger, A. L., Nelson, D. L., & Cox, M. M. (2005). *Lehninger principles of biochemistry*. Macmillan.

Li, Z. L., Wang, Z. J., Wei, G. H., Yang, Y., & Wang, X. W. (2020). Changes in extracellular matrix in different stages of colorectal cancer and their effects on proliferation of cancer cells. *World Journal of Gastrointestinal Oncology, 12*(3), 267–275. https://doi.org/10.4251/wjgo.v12.i3.267

Liu, H., Wang, Y., Cui, K., Guo, Y., Zhang, X., & Qin, J. (2019). Advances in hydrogels in organoids and organs-on-a-chip. *Advanced Materials, 31*(50), Article e1902042. https://doi.org/10.1002/adma.201902042

Liu, Y., Guan, Y., & Zhang, Y. (2015). Chitosan as inter-cellular linker to accelerate multicellular spheroid generation in hydrogel scaffold. *Polymer, 77*, 366–376.

Long, J., Etxeberria, A. E., Nand, A. V., Bunt, C. R., Ray, S., & Seyfoddin, A. (2019). A 3D printed chitosan-pectin hydrogel wound dressing for lidocaine hydrochloride delivery. *Materials Science and Engineering: C, 104*, Article 109873.

Mahboubian, A., Vllasaliu, D., Dorkoosh, F. A., & Stolnik, S. (2020). Temperature-responsive methylcellulose–hyaluronic hydrogel as a 3D cell culture matrix. *Biomacromolecules, 21*(12), 4737–4746.

Martins, J. G., Camargo, S. E., Bishop, T. T., Popat, K. C., Kipper, M. J., & Martins, A. F. (2018). Pectin-chitosan membrane scaffold imparts controlled stem cell adhesion and proliferation. *Carbohydrate Polymers, 197*, 47–56.

Matricardi, P., Di Meo, C., Coviello, T., Hennink, W. E., & Alhaique, F. (2013). Interpenetrating polymer networks polysaccharide hydrogels for drug delivery and tissue engineering. *Advanced Drug Delivery Reviews, 65*(9), 1172–1187.

Michailidou, G., Terzopoulou, Z., Kehagia, A., Michopoulou, A., & Bikiaris, D. N. (2021). Preliminary evaluation of 3D printed chitosan/pectin constructs for biomedical applications. *Marine Drugs, 19*(1), 36.

Nebuloni, M., Albarello, L., Andolfo, A., Magagnotti, C., Genovese, L., Locatelli, I., … Allevi, R. (2016). Insight on colorectal carcinoma infiltration by studying perilesional extracellular matrix. *Scientific Reports, 6*(1), 1–13.

Neufeld, L., & Bianco-Peled, H. (2017). Pectin–chitosan physical hydrogels as potential drug delivery vehicles. *International Journal of Biological Macromolecules, 101*, 852–861.

Neves, S. C., Gomes, D. B., Sousa, A., Bidarra, S. J., Petrini, P., Moroni, L., … Granja, P. L. (2015). Biofunctionalized pectin hydrogels as 3D cellular microenvironments. *Journal of Materials Chemistry B, 3*(10), 2096–2108. https://doi.org/10.1039/c4tb00885e

Nordby, M. H., Kjoniksen, A. L., Nystrom, B., & Roots, J. (2003). Thermoreversible gelation of aqueous mixtures of pectin and chitosan. Rheology. *Biomacromolecules, 4*(2), 337–343. https://doi.org/10.1021/bm020107+

Paschos, K. A., Canovas, D., & Bird, N. C. (2009). The role of cell adhesion molecules in the progression of colorectal cancer and the development of liver metastasis. *Cellular Signalling, 21*(5), 665–674. https://doi.org/10.1016/j.cellsig.2009.01.006

Quarta, A., Gallo, N., Vergara, D., Salvatore, L., Nobile, C., Ragusa, A., & Gaballo, A. (2021). Investigation on the composition of agarose–collagen I blended hydrogels as matrices for the growth of spheroids from breast cancer cell lines. *Pharmaceutics, 13*(7), 963.

Rangel, F. J. O. (2015). *Cell-laden micropatterns using self-assembled cell-ECM microtissues in soft pectin hydrogels*.

Reidy, E., Leonard, N. A., Treacy, O., & Ryan, A. E. (2021). A 3D view of colorectal cancer models in predicting therapeutic responses and resistance. *Cancers (Basel), 13*(2). https://doi.org/10.3390/cancers13020227

Sahu, A., Choi, W. I., & Tae, G. (2012). A stimuli-sensitive injectable graphene oxide composite hydrogel. *Chemical Communications, 48*(47), 5820–5822.

Shitrit, Y., Davidovich-Pinhas, M., & Bianco-Peled, H. (2019). Shear thinning pectin hydrogels physically cross-linked with chitosan nanogels. *Carbohydrate Polymers, 225*, Article 115249.

Siegel, R. L., Miller, K. D., Goding Sauer, A., Fedewa, S. A., Butterly, L. F., Anderson, J. C., … Jemal, A. (2020). Colorectal cancer statistics, 2020. *CA: A Cancer Journal for Clinicians, 70*(3), 145–164. https://doi.org/10.3322/caac.21601

Sigaeva, N., Vil'danova, R., Sultanbaev, A., & Ivanov, S. (2020). Synthesis and properties of chitosan-and pectin-based hydrogels. *Colloid Journal, 82*, 311–323.

Skardal, A., Devarasetty, M., Rodman, C., Atala, A., & Soker, S. (2015). Liver-tumor hybrid organoids for modeling tumor growth and drug response in vitro. *Annals of Biomedical Engineering, 43*(10), 2361–2373. https://doi.org/10.1007/s10439-015-1298-3

Stanzione, A., Polini, A., La Pesa, V., Romano, A., Quattrini, A., Gigli, G., … Gervaso, F. (2020). Development of injectable thermosensitive chitosan-based hydrogels for cell encapsulation. *Applied Sciences, 10*(18), 6550. https://doi.org/10.3390/app10186550

Supper, S., Anton, N., Seidel, N., Riemenschnitter, M., Schoch, C., & Vandamme, T. (2013). Rheological study of chitosan/polyol-phosphate systems: Influence of the polyol part on the thermo-induced gelation mechanism. *Langmuir, 29*(32), 10229–10237.

Tchoryk, A., Taresco, V., Argent, R. H., Ashford, M., Gellert, P. R., Stolnik, S., … Garnett, M. C. (2019). Penetration and uptake of nanoparticles in 3D tumor spheroids. *Bioconjugate Chemistry, 30*(5), 1371–1384.

Tentor, F. R., de Oliveira, J. H., Scariot, D. B., Lazarin-Bidóia, D., Bonafé, E. G., Nakamura, C. V., … Martins, A. F. (2017). Scaffolds based on chitosan/pectin thermosensitive hydrogels containing gold nanoparticles. *International Journal of Biological Macromolecules, 102*, 1186–1194. https://doi.org/10.1016/j.ijbiomac.2017.04.106

Thakuri, P. S., Liu, C., Luker, G. D., & Tavana, H. (2018). Biomaterials-based approaches to tumor spheroid and organoid modeling. *Advanced Healthcare Materials, 7*(6), Article e1700980. https://doi.org/10.1002/adhm.201700980

Torpol, K., Sriwattana, S., Sangsuwan, J., Wiriyacharee, P., & Prinyawiwatkul, W. (2019). Optimising chitosan–pectin hydrogel beads containing combined garlic and holy basil essential oils and their application as antimicrobial inhibitor. *International Journal of Food Science & Technology, 54*(6), 2064–2074.

Ventura, I., & Bianco-Peled, H. (2015). Small-angle X-ray scattering study on pectin–chitosan mixed solutions and thermoreversible gels. *Carbohydrate Polymers, 123*, 122–129.

Wang, C., Tong, X., & Yang, F. (2014). Bioengineered 3D brain tumor model to elucidate the effects of matrix stiffness on glioblastoma cell behavior using PEG-based hydrogels. *Molecular Pharmaceutics, 11*(7), 2115–2125.

Wieringa, P. A., Goncalves de Pinho, A. R., Micera, S., van Wezel, R. J. A., & Moroni, L. (2018). Biomimetic architectures for peripheral nerve repair: A review of biofabrication strategies. *Advanced Healthcare Materials, 7*(8), Article e1701164. https://doi.org/10.1002/adhm.201701164

Yan, Z., Chen, X., Liu, L., & Cao, X. (2019). Molecular interactions between some amino acids and a pharmaceutically active ionic liquid domiphen DL-mandelic acid in aqueous medium at temperatures from 293.15 K to 313.15 K. *The Journal of Chemical Thermodynamics, 138*, 1–13.

Yao, T., & Asayama, Y. (2017). Animal-cell culture media: History, characteristics, and current issues. *Reproductive Medicine and Biology, 16*(2), 99–117.

Zanoni, M., Cortesi, M., Zamagni, A., Arienti, C., Pignatta, S., & Tesei, A. (2020). Modeling neoplastic disease with spheroids and organoids. *Journal of Hematology & Oncology, 13*(1), 97. https://doi.org/10.1186/s13045-020-00931-0

Zhou, H. Y., Jiang, L. J., Cao, P. P., Li, J. B., & Chen, X. G. (2015). Glycerophosphate-based chitosan thermosensitive hydrogels and their biomedical applications. *Carbohydrate Polymers, 117*, 524–536. https://doi.org/10.1016/j.carbpol.2014.09.094